Effect of reduced saturation and elevated D-dimer and interleukin 6 levels on vessel density and foveal avascular zone in patients with COVID-19 bilateral pneumonia

Magdalena Kal^{1,2,A–F}, Michał Brzdęk^{3,1,D–F}, Elżbieta Cieśla^{4,C,E,F}, Piotr Rzymski^{5,E,F}, Izabella Karska-Basta^{6,A,D–F}, Antonio Pinna^{7,A,E,F}, Jerzy Mackiewicz^{8,A,D–F}, Mateusz Winiarczyk^{8,A,D–F}, Dominik Odrobina^{2,9,A,E,F}, Dorota Zarębska-Michaluk^{1,3,A,E,F}

- ¹ Collegium Medicum of Jan Kochanowski University in Kielce, Poland
- ² Ophthalmic Clinic of the Voivodeship Hospital in Kielce, Poland
- ³ Department of Infectious Diseases and Allergology, Jan Kochanowski University in Kielce, Poland
- ⁴ Institute of Health Sciences, Jan Kochanowski University in Kielce, Poland
- ⁵ Department of Environmental Medicine, Poznan University of Medical Sciences, Poland
- 6 Department of Ophthalmology, Clinic of Ophthalmology and Ocular Oncology, Faculty of Medicine, Jagiellonian University Medical College, Cracow, Poland
- ⁷ Department of Medicine, Surgery, and Pharmacy, Ophthalmology Unit, University of Sassari, Italy
- ⁸ Department of Vitreoretinal Surgery, Medical University of Lublin, Poland
- ⁹ Insitute of Medical Science, Jan Kochanowski University in Kielce, Poland
- A research concept and design; B collection and/or assembly of data; C data analysis and interpretation;
- D writing the article; E critical revision of the article; F final approval of the article

Advances in Clinical and Experimental Medicine, ISSN 1899-5276 (print), ISSN 2451-2680 (online)

Adv Clin Exp Med. 2025;34(8):1331-1342

Address for correspondence

Michał Brzdęk E-mail: michal.brzdek@gmail.com

Funding sources

None declared

Conflict of interest

None declared

Received on October 23, 2023 Reviewed on March 16, 2024 Accepted on July 29, 2024

Published online on November 7, 2024

Cite as

Kal M, Brzdęk M, Cieśla E, et al. Effect of reduced saturation and elevated D-dimer and interleukin-6 levels on vessel density and foveal avascular zone in patients with COVID-19 bilateral pneumonia. *Adv Clin Exp Med*. 2025;34(8):1331–1342. doi:10.17219/acem/191774

DOI

10.17219/acem/191774

Copyright

Copyright by Author(s)
This is an article distributed under the terms of the
Creative Commons Attribution 3.0 Unported (CC BY 3.0)
(https://creativecommons.org/licenses/by/3.0/)

Abstract

Background. Severe acute respiratory syndrome coronavirus 2 (SARS-CoV-2) infection can affect multiple organs, including the eyes.

Objectives. This study aimed to identify associations between vascular density (VD) and the foveal avascular zone (FAZ), assessed using optical coherence tomography angiography (OCTA), and baseline levels of D-dimers and interleukin 6 (IL-6) in patients with bilateral COVID-19 pneumonia, depending on oxygen saturation (SpO_2) on admission.

Materials and methods. The study included patients with COVID-19 bilateral pneumonia due to SARS-CoV-2 infection who were hospitalized between March and May 2021. Ophthalmological examination was performed 2 months after hospitalization. Optical coherence tomography angiography was used for the automatic assessment of the central retinal VD and the manual assessment of FAZ.

Results. A significant monotonic negative relationship was observed between $SpO_2 \le 90\%$ and VD in some areas of the superficial capillary plexus (SCP) (p = 0.048) and choriocapillaris (p = 0.021), and the mean VD in the deep capillary plexus (DCP) (p = 0.048). No significant monotonic negative relationship was noted between $SpO_2 \le 90\%$ and the FAZ in the SCP (p = 0.075). However, there was a significant monotonic positive relationship between VD in the nasal choriocapillaris and D-dimer levels in patients with $SpO_2 \le 90\%$ (p = 0.003, respectively). Finally, a monotonic negative relationship was identified between foveal VD in the DCP and IL-6 levels in patients with $SpO_2 \le 90\%$ (p = 0.027).

Conclusions. An OCTA study conducted 2 months after hospitalization for COVID-19 bilateral pneumonia showed reduced VD in those with $SpO_2 \le 90\%$ and elevated levels of D-dimers and IL-6 during hospitalization. Optical coherence tomography angiography testing can provide monitoring of ocular status in patients following SARS-CoV-2 infection, especially those who report visual disturbances.

Key words: vessel density, oxygen saturation, COVID-19, optical coherence tomography angiography, foveal avascular zone

Background

Severe acute respiratory syndrome coronavirus 2 (SARS-CoV-2) is a virus that was initially identified in the airway epithelium of patients with pneumonia in Wuhan, China, in 2019. In March 2020, SARS-CoV-2 infection grew into a global pandemic. The virus causes coronavirus disease 2019 (COVID-19) with a wide spectrum of clinical pictures. Disease severity ranges from mild to fatal, depending on the virus itself and the patient's immune response.

Immune hyperreactivity leads to a cytokine storm with extensive vascular endothelial damage, increased blood clotting and overproduction of inflammatory factors. The lungs are the main site of the clinical manifestation of COVID-19, but other organs are also involved, including the kidneys, intestines, brain, heart, and eyes. One of the main cytokines participating in the pathogenesis of cytokine storm is interleukin 6 (IL-6).

SARS-CoV-2 infection is mediated by the viral protein binding to the angiotensin-converting enzyme 2 (ACE2) receptor, which is responsible for the viral cellular entry. After attaching to ACE2, transmembrane serine protease 2 cleaves and stimulates the receptor-bound viral spike protein, thereby mediating the fusion of the viral envelope with the membrane of the target cell in the host.9 The ACE2 is found on the surface of almost all vascular endothelial cells (VECs). When bound to SARS-CoV-2, it activates the rennin-angiotensin system, which reduces ACE2 expression and increases angiotensin II levels. Angiotensin II causes vasoconstriction and elevates the levels of tissue factor and plasminogen activator inhibitor, resulting in thrombosis. Angiotensin also participates in complement activation by generating reactive oxygen species (ROS) and downregulating C1 inhibitors. This, in turn, leads to increased vessel permeability and the release of cytokines, thereby increasing the thrombotic effects of angiotensin.¹⁰ Patients with COVID-19 show generalized microvascular thrombosis and elevated Ddimer levels.11

Optical coherence tomography angiography (OCTA) is a useful tool for a noninvasive assessment of the microvasculature in the central retina and choroid of the eye. It enables the measurement of such parameters as vascular density (VD) and foveal avascular zone (FAZ) in patients with various systemic disorders such as anemia, carotid stenosis and SARS-CoV-2 infection. OCTA parameters between healthy controls and COVID-19 patients hospitalized for bilateral pneumonia. These differences persisted for at least 6 months. 15,16

Objectives

This study aimed to identify associations of the OCTA parameters VD and FAZ with baseline oxygen saturation

(SpO₂), D-dimer levels and IL-6 levels in patients with COVID-19 bilateral pneumonia.

Materials and methods

Study design

This prospective study was conducted in the Department of Infectious Diseases and the Ophthalmology Clinic of the Provincial Hospital in Kielce, Poland, from March to May 2021. The study was approved by the Bioethics Committee of the Collegium Medicum of Jan Kochanowski University in Kielce (study code 54; July 1, 2021). It was conducted in accordance with the Declaration of Helsinki, and all patients gave their informed consent.

Setting

While under SARS-CoV-2 infection, all patients were treated in the Department of Infectious Diseases. Two months after hospital discharge, they were examined in the Ophthalmology Clinic. In all patients, COVID-19 bilateral pneumonia was caused by the B.1.1.7 variant of SARS-CoV-2. The infection was determined by a positive polymerase chain reaction (PCR) test or a COVID-19 antigen rapid test device (Abbott, Lake Country, USA) Pneumonia was confirmed based on the presence of typical lesions on computed tomography (CT). The current study reports the outcomes of patients with COVID-19 bilateral pneumonia at 2 months after hospital discharge. The in-hospital outcomes of the study have been reported previously. 15

Participants

The following exclusion criteria were applied: myopia higher than -3 diopters, hyperopia higher than +3 diopters, retinal diseases, optic neuropathies, previous eye surgery, uveitis, ocular injury, opaque media affecting OCTA scan or image quality, and diabetes mellitus.

Of the 94 patients (188 eyes) initially enrolled in the study, we excluded those with age-related macular degeneration (n = 10), diabetes mellitus (n = 13), glaucoma (n = 2), high hyperopia (n = 1), high myopia (n = 3), previous cataract surgery (n = 2), and poor-quality OCTA images (n = 1). Among the remaining 62 patients (124 eyes), we excluded 2 eyes with hyperopia >3 diopters, 1 eye with myopia >3 diopters, 1 eye after ocular trauma, and 1 eye after uveitis.

Variables

Baseline patient characteristics included demographic and clinical data: sex, age, body mass index (BMI), visual acuity, reading vision, spherical equivalent, axial length, and oxygen saturation (SpO₂). Baseline laboratory parameters included serum alanine transaminase (ALT) activity, concentrations of C-reactive protein (CRP), procalcitonin (PCT), IL-6, D-dimer, white blood cell count (WBC), lymphocyte count, neutrophil count, and platelet count. In this study, we gathered crucial data pertaining to COVID-19 treatment, including the administration of low-molecular-weight heparin (LMWH) in both prophylactic and therapeutic doses; administration of tocilizumab, dexamethasone and remdesivir; and the need for continuous oxygen therapy. We conducted an assessment of VD and FAZ using OCTA.

Measurement

Optical coherence tomography angiography was performed using a TopconSwept Source DRIOCT Triton device (Topcon Inc., Tokyo, Japan). The images were captured using the 4.5×4.5 mm and 6×6 mm scanning protocols. Central retinal parameters were obtained using the Early Treatment Diabetic Retinopathy Study (ETDRS) grid consisting of 3 concentric circles with diameters of 1, 3 and 6 mm.

Vascular density was assessed in the superficial capillary plexus (SCP), deep capillary plexus (DCP) and choriocapillaris (CC), using the EDTRS grid subfield to define the areas of interest. The 5 areas of VD were defined as foveal VD, superior VD, nasal VD, inferior VD, and temporal VD. The VD values obtained in the parafoveal area (superior, nasal and inferior) were added together, and the average value was calculated to obtain mean VD.

The FAZ area is the central part of the macula without visible vessels (Fig. 1). Two independent ophthalmologists

delineated the FAZ manually on the SCP and the DCP. Optical coherence tomography angiography scans with a quality of over 65% were eligible for examination.

Oxygen saturation, D-dimer levels and IL-6 levels assessed on admission for COVID-19 bilateral pneumonia were retrospectively obtained from hospital records. We assessed the correlations of baseline D-dimer, IL-6 and SpO_2 levels with the OCTA parameters VD and FAZ.

Statistical analyses

We calculated the frequencies (n) and percentages (%) for qualitative variables such as gender, use of drugs and the need for continuous oxygen therapy. Distributions were estimated for quantitative variables such as saturation, D-dimers, IL-6, and VD in the SCP, DCP, CC, and FAZ areas (Supplementary Fig. 1-82). Subsequently, the arithmetic mean and standard deviation (SD) or median (Me) and interquartile range (IQR) were calculated, depending on the distribution of the variables. Calculations were performed for the entire group and within groups for saturation (SpO₂ \leq 90%, 91–95% and >95%), IL-6 (≤1.8 pg/mL and >1.8 pg/mL) and D-dimers (>500 µg/land and ≤500µg/L). Depending on whether data met the assumptions of Gaussian distribution and homogeneity of variance, the parametric Student's t-test or the non-parametric Mann–Whitney U test was used to assess differences in groups distinguished by IL-6 and D-dimers. Similarly, the parametric analysis of variance (ANOVA) test or the non-parametric Kruskal-Wallis ANOVA wasemployed to assess differences in means in saturation groups. Bonferroni corrections were applied to any multiple comparisons

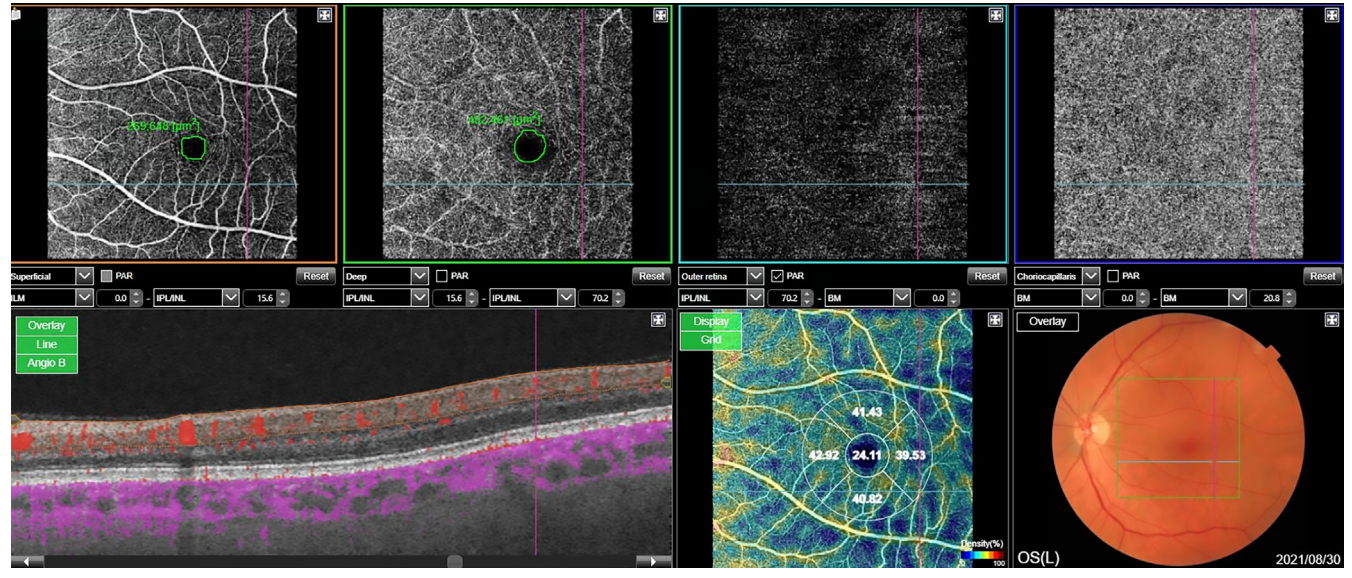


Fig. 1. The image of the foveal avascular zone (FAZ) was obtained using optical coherence tomography angiography (OCTA) manually: in the superficial capillary plexus (SCP) (left, superior corner) and in the deep capillary plexus (DCP) (the image next to the image of SCP) in the left eye. The map of the vessel density (VD) in the left eye was assessed automatically with OCTA using the early treatment diabetic retinopathy (ETDRS) grid situated in the fovea by fixation (right, lower corner) The automatic map of central VD is divided into 5 areas: the foveal VD (F VD = 24.11%), the superior area (S VD = 41.43%), the inferior VD (I VD = 40.82%), the temporal VD (T VD = 39.53%), and the nasal VD (N VD = 42.92%)

to account for alpha inflation and limit the probability of type 1 error (Supplementary Tables 1–3). The linearity was assessed based on scatter plots between saturation values, D-dimers, IL-6, and ocular parameters (Supplementary Fig. 83-143). Spearman rank correlation coefficients were used to assess the significance, direction and strength of the monotonic component of the relationship with VD in the SCP, DCP, CC, and FAZ areas based on OCTA and levels of D-dimers and IL-6 according to the saturation groups: $SpO_2 \le 90\%$, 91–95% and >95%. Correlations were interpreted using Guilford's classification. The assumptions of the Student's t-tests were verified (testing the normality of distributions within groups with the Shapiro-Wilk test and the homogeneity of variances with Levene'stest). The same procedure was applied for the ANOVA. In case of heterogeneity of variances, Welch's F test was employed (Supplementary Table 1). Additionally, the difference (d) between individual means was calculated, and effect size was computed for all parameters in the saturation and D-dimer groups. For the Kruskal-Wallis ANOVA test, the following formula was used: eta2[H] = (H - k)+ 1)/(n - k), where H represents the value obtained in the Kruskal-Wallis test, k is the number of groups and n is the total number of observations. For the Student's t-test, Cohen's D was calculated according to the formula $D = (mean1 - mean2)/sd_pooled$. For the Mann-Whitney test, the Wendt formula was applied: It computes the rank-biserial correlation from U and from the sample size (n) of the 2 groups: $r = 1 - (2U)/(n1 \times n2)$. Here, U denotes the value of the U parameter, n1 is the number for the 1st group, and n2 is the number for the 2nd group. In the parametric ANOVA test, eta square was employed as the measure of effect size; it was calculated according to the formula Eta squared = SSeffect/SStotal. The qualitative variables were presented as frequencies and percentages. A p-value of less than 0.05 was considered significant. Statistical analyses were done using Statistica v. 13.3 (StatSoft Poland, Cracow, Poland).

Results

Study group

The final study group included 119 eyes of 62 patients (42 men (67.7%) and 20 women (32.3%); mean age, 51.33 ± 1.30 years). Patients were classified into 3 groups depending on SpO₂ at baseline: >95% (n = 22), 91–95% (n = 29) and \leq 90% (n = 11). The demographic and ocular characteristics of patients are presented in Table 1.

Table 1. Demographic and ocular characteristics of patients with COVID-19 bilateral pneumonia

Variable		Value
Men, n (%)		42 (68.25)
Women, n (%)		20 (31.75)
Age [years] ^a	mean (SD)	51.33 (1.30)
BMI [kg/m²]b	mean (SD)	28.41 (4.07)
Visual acuity*,c	median (IQR)	0.5 (0.0)
Reading vision*,d	median (IQR)	0.3 (0.0)
Spherical equivalent [diopters]e	mean (SD)	0.13 (0.13)
Axial length [mm] ^f	mean (SD)	23.55 (0.8)
	median (IQR)	23.45 (1.05)

*Based on the LogMar scale. BMI – body mass index; SD – standard deviation; IQR – interquartile range; ^aShapiro–Wilk-test: p = 0.127; ^bShapiro–Wilk-test: p = 0.817; ^cShapiro–Wilk-test: p < 0.001; ^aShapiro–Wilk-test: p = 0.171; ^cShapiro–Wilk-test: p = 0.514.

Visual acuity and laboratory and imaging tests on admission

Visual acuity and reading vision were assessed using the LogMar scale. The means for visual acuity and reading vision at 2 months after discharge are presented in Table 1.

Laboratory test results on admission, including mean SpO₂, CRP, PCT, WBC, lymphocytes, neutrophils, platelets, IL-6, D-dimers, and ALT, are presented in Table 2. Bilateral

Table 2. Baseline laboratory parameters in COVID-19 patients

Variable	Mean (SD)	Q1-Q3	Reference range
SpO ₂ [%]	93.34 (3.68)	92.0–96.0	>95%
CRP [mg/dL]	63.99 (65.20)	14.58–93.42	<1.0
PCT [ng/mL]	0.17 (0.25)	0.04-0.18	0.05-0.1
WBC [µL]	5,723.23 (2312.33)	4,332.50-6,337.50	4,000-10,000
Lymphocytes [µL]	1,222.26 (416.43)	910.0–1,472.50	1,000–5,000
Neutrophils [μL]	3,997.26 (2,078.68)	2,532.5–4666.0	1,800–8,000
Platelets [µL]	205,411.29 (68,271.24)	150,500.0-231,000.0	150,000–400,000
IL-6 [pg/mL]	35.79 (27.75)	13.02-48.48	1.22 ±0.706
D-dimer [µg/L]	1,095.29 (3,435.20)	387.5–700.5	<500
ALT [U/L]	56.45 (37.45)	26.25–73.25	5–40

lung lesions were confirmed with chest CT as ground glass opacities in 26 patients during hospitalization.

Treatment of COVID-19 patients during hospitalization

Study participants hospitalized due to SARS-CoV-2 infection were treated in line with applicable recommendations.¹⁷ Oxygen supplementation was used in 23 patients for a median (Q1–Q2) (Table 3). In 59 patients, LMWH was administered at a prophylactic dose depending on body weight according to the summary of product characteristics. During the viral phase of COVID-19, 26 subjects were treated with intravenous remdesivir. The initial dose was 200 mg on the 1st day, followed by 100 mg for the next 4 days. Patients with hyperinflammatory syndrome were treated with immunosuppressive drugs. Dexamethasone was used on 22 patients (4 mg/day orally or 8 mg/day intravenously for 7–10 days). Intravenous tocilizumab was given to 3 patients at a single dose of 600-800 mg, depending on the patient's weight, according to the summary of product characteristics and national recommendations. Tocilizumab was administered in patients with elevated IL-6 levels.18

Table 3. Systemic treatment for COVID-19

Treatment	Value
Low-molecular-weight heparin, prophylactic dose, n (%)	59 (95.16)
Low-molecular-weight heparin, prophylactic dose, number of days: median (Q1–Q3)	9 (6.25–12)
Low-molecular-weight heparin, therapeutic dose, n (%)	2 (3.23)
Tocilizumab, n (%)	3 (4.84)
Dexamethasone, n (%)	22 (35.48)
Remdesivir, n (%)	26 (41.94)
Need for continuous oxygen therapy, n (%)	23 (37.10)
Need for continuous oxygen therapy, number of days, median (Q1–Q3); min–max	5 (4–10); 1–26

Q – quartile.

Structural OCTA outcomes depending on oxygen saturation and D-dimer and IL-6 levels

Differences in ocular parameters were observed in the OCTA scans depending on saturation levels. Post hoc analysis indicated significant differences between saturation groups 1 and 3, and between groups 2 and 3. Less frequent were differences based on the D-dimer and IL-6 groups (Supplementary Tables 1–3).

At 2 months, a significant monotonic negative relationship was found between SpO_2 of 90% or lower and VD in the foveal area of the SCP and the temporal area

of the choriocapillaris (CC) and mean VD in the DCP (Table 4). Furthermore, there was a significant monotonic positive relationship between D-dimer levels in patients with SpO_2 of 90% or lower and VD in the nasal choriocapillaris CC (Table 4). Lastly, a monotonic negative relationship was identified between foveal VD in the DCP and IL-6 levels in patients with SpO_2 of 90% or lower (Table 4).

Safety

In the study group, hypertension was reported in 20 patients, ischemic heart disease in 3, fatty liver disease in 5, hyperlipidemia in 3, previous stroke in 2, previous myocardial infarction in 2, cancer in 5, degenerative spine disease in 2, hyperthyroidism in 2, and hysterectomy in 2. Asthma, epilepsy, delusional disorder, rheumatoid arthritis, chronic kidney disease (CKD), nephrolithiasis, chronic hepatitis C, cholelithiasis, thyroidectomy, and alcohol dependence were reported in 1 patient each. No patients reported any symptoms during the ophthalmological examination.

Discussion

The SARS-CoV-2 infection primarily affects the respiratory tract, but it also causes inflammation in the vascular endothelium with strong cytokine involvement, resulting in enhanced clotting in the microcirculation.¹⁹

Numerous papers have described fundus lesions caused by COVID-19.^{20–23} These abnormalities, including hemorrhages and cotton wool spots, are typical for central retinal vein occlusion with subsequent macular edema. This indicates that the disease is vascular in nature. Noninvasive tests such as OCTA have been repeatedly used to diagnose the above conditions.

To demonstrate the effect of systemic hypoxia on retinal and choroidal microvasculature assessed using OCTA, we followed the same approach as our previous study: We divided COVID-19 patients into subgroups according to SpO₂ on admission.²⁴

In the present study, we assessed correlations between SpO_2 , D-dimer and IL-6 levels and ocular parameters such as VD and FAZ area as obtained using OCTA in patients with SARS-CoV-2 infection, at 2 months after hospital discharge. The aim of the study was to evaluate whether hypoxia, inflammation and hypercoagulability affect the retinal and choroidal microvasculature.

Correlations between SpO₂ and VD

Our study showed a significant monotonic negative relationship between SpO_2 of 90% or lower and VD in the foveal SCP and temporal CC, and the mean VD in the DCP.

Hommer et al.²⁵ evaluated the effects of hypoxia in 24 healthy subjects (mean age 26 years) on vasculature parameters in the central retina obtained with

Table 4. Correlations between vessel density in the superficial capillary plexus (SCP), deep capillary plexus (DCP), and choriocapillaris (CC) and foveal avascular zone (FAZ) in the SCP and DCP and oxygen saturation (SpO₂), interleukin 6 (IL-6) levels and D-dimer levels

ОСТА	SpO ₂	D-dimer	IL-6
Foveal VD in the SCP	r = -0.22; p = 0.048	r = -0.06; p = 1	r = −0.06; p = 1
Foveal VD in the DCP	r = -0.13; p = 0.513	r = -0.06; p = 1	$r = -0.10$; $p = 0.786$ for $SpO_2 \le 90\%$ r = -0.57, $p = 0.027$
Foveal VD in the CC	r = -0.11; $p = 0.645$	$r = 0.04$; $p = 1$ for $SpO_2 \le 90\%$ r = 0.33; $p = 0.06$	r = 0.17; p = 0.216
Superior VD in the SCP	r = 0.08; p = 1	r = -0.13; p = 0.486	r = 0.01; p = 1
Superior VD in the DCP	r = -0.01; $p = 1$	r = -0.11; $p = 0.729$	r = -0.06; p = 1
Superior VD in the CC	r = -0.01; p = 1	r = 0.08; p = 1	r = -0.01; p = 1
Nasal VD in the SCP	r = 0.11; p = 0.624	r = -0.11; $p = 0.72$	r = 0.08; p = 1
Nasal VD in the DCP	r = 0.01; p = 1	$r = -0.17$; $p = 0.183$ for $SpO_2 \le 90\%$ r = -0.32; $p = 0.288$	r = 0.10; p = 0.906
Nasal VD in the CC	r = -0.05; p = 1	$r = -0.07$; $p = 1$ for $SpO_2 \le 90\%$ r = 0.49; $p = 0.003$	r = 0.03; p = 1
Inferior VD in the SCP	r = 0.13; p = 0.525	r = 0.05; p = 1	r = -0.05; p = 1
Inferior VD in the DCP	r = -0.08; $p = 1$	r = -0.05; $p = 1$	r = 0.15; p = 0.321
Inferior VD in the CC	r = -0.08; p = 1	$r = 0.16$; $p = 0.237$ for $SpO_2 \le 90\%$ r = -0.36; $p = 0.054$	r = -0.06; p = 1
Temporal VD in the SCP	r = 0.07; p = 1	r = -0.04; $p = 1$	r = -0.14; p = 0.396
Temporal VD in the DCP	$r = -0.16$; $p = 0.255$ for $SpO_2 \le 90\%$ r = -0.47; $p = 0.135$	r = 0.07; p = 1	r = 0.06; p = 1
Temporal VD in the CC	$r = -0.12$; $p = 0.543$ for $SpO_2 \le 90\%$ r = -0.59; $p = 0.021$	r = 0.04; p = 1	r = 0.12; p = 0.618
Mean VD in the SCP	r = 0.02; p = 1	r = -0.09; p = 1	r = -0.01; p = 1
Mean VD in the DCP	$r = -0.15$; $p = 0.339$ for $SpO_2 \le 90\%$ r = -0.55; $p = 0.048$	r = -0.12; p = 0.546	r = 0.01;p = 1
Mean VD in the CC	r = -0.14; p = 0.345	r = 0.17; p = 0.174	r = 0.08; p = 1
FAZ in the SCP	r = −0.20; p = 0.075	r = -0.01; $p = 1$	r = -0.06; p = 1
FAZ in the DCP	r = 0.13; p = 0.414	r = 0.09; p = 0.921	r = -0.08; $p = 1$

 $p\ for\ Sp-Spearman\ rank\ correlation; values\ were\ statistically\ significant\ at\ p<0.05; optical\ coherence\ tomography\ angiography\ (OCTA);\ VD-vascular\ density.$

OCTA while breathing a mixture of nitrogen (88%) and oxygen (12%). Perfusion density in the superficial vascular density was significantly elevated and was stable in the DCP. Retinal vessel diameter was also significantly increased. Moreover, significantly elevated perfusion density in the DCP was observed in patients breathing 100% oxygen. At the same time, a significant reduction in vessel diameter was noted in the major retinal arteries and veins.²⁵

For proper function, the retina requires an adequate oxygen supply. Retinal vessels can regulate blood circulation in response to hypoxia and hyperoxia. Hyperoxia reduces the caliber of retinal vessels. This regulatory mechanism helps avoid the oversupply of oxygen to the retina, which can induce retinal nerve fiber toxicity. The risk of hyperoxygenation and oxidative stress is reduced by the vasospasm of the vessels in the DCP.^{26,27}

Correlations between SpO₂ and FAZ area

The large number of cones and the absence of retinal vessels in the FAZ area allow the best vision. Therefore, this area is particularly sensitive to hypoxia. The CC layer under the retina is responsible for supplying oxygen and nutrients to the cones that are located here. The enlargement of the FAZ area may indicate abnormalities associated with vascular disorders such as diabetic retinopathy or retinal veinocclusion. However, in our study, there was no significant monotonic negative relationship between SpO₂ of 90% or lower and the FAZ area in the SCP and the DCP.

Correlations between D-dimer levels and VD

Our study showed a significant monotonic positive relationship between VD in the CC and D-dimer levels, but

only in patients with SpO_2 of 90% or lower in the nasal area of the CC.

Guemez-Villahoz et al. 30 reported reduced mean blood flow (19.6 \pm 9.3 vs 14.7 \pm 8.0, p = 0.018) and reduced VD in the SCP (8.8 \pm 4.0 vs 6.6 \pm 3.6, p = 0.013) 30 days after the diagnosis of COVID-19 in patients with elevated D-dimer levels of 500 ng/mL or higher. They hypothesized that the subclinical changes in the retinal microcirculation in these patients were secondary to increased blood clotting and intense inflammatory response due to COVID-19. 30

In a subsequent paper, Guemez-Villahoz et al.³¹ described OCTA outcomes at 12 weeks after the acute stage of COVID-19 in patients divided according to the presence of thrombotic events. They also compared OCTA findings between patients with COVID-19 and healthy controls. They found significantly reduced VD in patients with COVID-19 compared with controls in several areas of the macula, including the central macula, outer ring and full ring. Perfusion density was significantly reduced in the full ring and full area. Optical coherence tomography angiography parameters did not differ between the groups with and without thrombotic events. According to the authors, retinal vascular involvement in SARS-CoV-2 infection does not depend on the presence of thrombotic events at other levels. In addition, there were no retinal vascular incidents in COVID-19 patients with thrombotic events.³¹

Correlations between II-6 levels and VD

In our study, there was a significant monotonic negative relationship between VD in some areas of the DCP and IL-6 levels in patients with SpO_2 of 90% or lower.

To our knowledge, no previous studies have described correlations between OCTA parameters and interleukin levels in patients with SARS-CoV-2 infection. Nevertheless, IL-6 is known to be one of the main mediators in retinal vasculitis. Mesquida et al. 33 studied the effects of IL-6 on the retinal endothelium and retinal pigment epithelium (RPE) in vitro using human RPE cells and endothelial cells of the retinal vessels to show that this is the most important additional mediator of macular edema in numerous retinal diseases. Interleukin 6 impairs barrier function in RPE cells and retinal VECs. 33

Park et al.³⁴ used human monocytes to investigate the relationship between elevated D-dimer levels, immune complexes and inflammatory processes in patients with COVID-19. They showed that D-dimers stimulate prostaglandin E2 (PGE2) and inflammatory cytokines such as IL-6, IL-8 and IL-1 β in healthy monocytes. The monocytes were incubated with D-dimers and immune complexes of SARS-CoV-2 particles, resulting in a significant increase in PGE2 levels and cytokine production.³⁴ This confirmed the findings of other investigators who have emphasized the importance of the thrombolytic-inflammatory concept as a key phenomenon in the pathomechanism of COVID-19.^{35,36}

Limitations

Several limitations of this study should be acknowledged. First, for organizational and logistical reasons, patients were assessed 2 months after hospitalization for COVID-19 bilateral pneumonia and not during the hospitalization itself. Second, the study did not include critically ill patients who required intensive care admission due to progressive hypoxia, which is associated with releasing proinflammatory and prothrombotic factors that could affect retinal and choroidal microvascular parameters. Finally, the study group was relatively small. Further research on a larger group of patients should be conducted to provide more information on the effect of COVID-19 on the microvasculature of the retina and choroid.

Conclusions

Patients with COVID-19 bilateral pneumonia with reduced SpO_2 and elevated D-dimer and IL-6 levels present with decreased VD in some areas assessed by OCTA. These patients require particular attention during anatomical and functional evaluation of posterior ocular structures. Optical coherence tomography angiography is a useful and widely available tool for the diagnosis of vascular disorders in the central retina and choroid in patients with previous SARS-CoV-2 infection.

Supplementary data

The Supplementary materials are available at https://doi. org/10.5281/zenodo.12745888. The package includes the following files:

Supplementary Table 1. Means, SD, median and IQR for OCTA parameters in 3 groups saturation (group 1: \leq 90; group 2: 90-95; group 3: >95).

Supplementary Table 2. Characteristic of OCTA parameters according to D-dimers level group (>500 ng - group 0).

Supplementary Table 3. Characteristic of OCTA parameters according to IL-6 level (group 0: ≤1.8, group 1: >1.8).

Supplementary Fig. 1. The diagram for the correlation between VD F SCP (foveal vascular density in superficial capillary plexus) and saturation.

Supplementary Fig. 2. The diagram for the correlation between VD F DCP (foveal vascular density of deep capillary plexus) and saturation

Supplementary Fig. 3. The diagram for the correlation between VD F CC (foveal vascular density of choriocapillaris) and saturation.

Supplementary Fig. 4. The diagram for the correlation between VD S SCP (temporal vascular density of superficial capillary plexus) and saturation.

Supplementary Fig. 5. The diagram for the correlation between VD S DCP (superior vascular density of deep capillary plexus) and saturation.

Supplementary Fig. 6. The diagram for the correlation between VD S CC (superior vascular density of choriocapillaris) and saturation.

Supplementary Fig. 7. The diagram for the correlation between VD N SCP (nasal vascular density of superficial capillary plexus) and saturation.

Supplementary Fig. 8. The diagram for the correlation between VD N DCP (nasal vascular density of deep capillary plexus) and saturation.

Supplementary Fig. 9. The diagram for the correlation between VD N CC (nasal vascular density of choriocapillaris) and saturation.

Supplementary Fig. 10. The diagram for the correlation between VD I SCP and (inferior vascular density of superficial capillary plexus) and saturation.

Supplementary Fig. 11. The diagram for the correlation between VD I DCP (inferior vascular density of deep capillary plexus) and saturation.

Supplementary Fig. 12. The diagram for the correlation between VD I CC (inferior vascular density of choriocapillaris) and saturation.

Supplementary Fig. 13. The diagram for the correlation between VD T SCP (temporal vascular density of superficial capillary plexus) and saturation.

Supplementary Fig. 14. The diagram for the correlation between VD T DCP (temporal vascular density of deep capillary plexus) and saturation.

Supplementary Fig. 15. The diagram for the correlation between $VD\ T\ CC$ (temporal vascular density of choriocapillaris) and saturation.

Supplementary Fig. 16. The diagram for the correlation between mean VD SCP (vascular density of superficial capillary plexus) and saturation.

Supplementary Fig. 17. The diagram for the correlation between mean VD DCP (vascular density of deep capillary plexus) and saturation.

Supplementary Fig. 18. The diagram for the correlation between mean VD CC (vascular density of choriocapillaris) and saturation.

Supplementary Fig. 19. The diagram for the correlation between FAZs (μm^2) (superficial foveal avascular zone) and saturation.

Supplementary Fig. 20. The diagram for the correlation between FAZd (μm^2) (deep foveal avascular zone) and saturation.

Supplementary Fig. 21. The diagram for the correlation between VD F SCP (foveal vascular density of superficial capillary plexus) and IL-6 level.

Supplementary Fig. 22. The diagram for the correlation between VD F DCP (foveal vascular density of deep capillary plexus) and IL-6 level.

Supplementary Fig. 23. The diagram for the correlation between VD F CC (foveal vascular density of choriocapillaris) and IL-6 level.

Supplementary Fig. 24. The diagram for the correlation between VD S SCP (superior vascular density of superficial capillary plexus) and IL-6 level.

Supplementary Fig. 25. The diagram for the correlation between VD S DCP (superior vascular density of deep capillary plexus) and IL-6 level.

Supplementary Fig. 26. The diagram for the correlation between VD N SCP (nasal vascular density of superficial capillary plexus) and IL-6 level.

Supplementary Fig. 27. The diagram for the correlation between VD S CC (superior vascular density of choriocapillaris) and IL-6 level.

Supplementary Fig. 28. The diagram for the correlation between VD N DCP (nasal vascular density of deep capillary plexus) and IL-6 level.

Supplementary Fig. 29. The diagram for the correlation between VD N CC (nasal vascular density of choriocapillaris) and IL-6 level.

Supplementary Fig. 30. The diagram for the correlation between VD I SCP (inferior vascular density of superficial capillary plexus) and IL-6 level.

Supplementary Fig. 31. The diagram for the correlation between VD I DCP (inferior vascular density of deep capillary plexus) and IL-6.

Supplementary Fig. 32. The diagram for the correlation between VD I CC (inferior vascular density of choriocapillaris) and IL-6 level.

Supplementary Fig. 33. The diagram for the correlation between VD T SCP (temporal vessel density of superficial capillary plexus) and IL-6 level.

Supplementary Fig. 34. The diagram for the correlation between VD T DCP (temporal vessel density of deep capillary plexus) and IL-6 level.

Supplementary Fig. 35. The diagram for the correlation between VD T CC (temporal vessel density of choriocapillaris) and IL-6 level.

Supplementary Fig. 36. The diagram for the correlation between mean VD SCP (vessel density of superficial capillary plexus) and IL-6 level.

Supplementary Fig. 37. The diagram for the correlation between mean VD DCP (vessel density of deep capillary plexus) and IL-6 level.

Supplementary Fig. 38. The diagram for the correlation between mean VD CC (vessel density of choriocapillaris) and IL-6 level.

Supplementary Fig. 39. The diagram for the correlation between FAZs (superficial foveal avascular zone) and IL-6 level.

Supplementary Fig. 40. The diagram for the correlation between FAZd (deep foveal avascular zone) and IL-6 level.

Supplementary Fig. 41. The diagram for the correlation between VD F SCP (foveal vessel density of superficial capillary plexus) and D-dimers level.

Supplementary Fig. 42. The diagram for the correlation between VD F DCP (foveal vessel density of deep capillary plexus) and D-dimers level.

Supplementary Fig. 43. The diagram for the correlation between VD F CC (foveal vessel density of choriocapillaris) and D-dimers level.

Supplementary Fig. 44. The diagram for the correlation between VD S SCP (vessel density of superficial capillary plexus) and D-dimers level.

Supplementary Fig. 45. The diagram for the correlation between VD S DCP (superior vessel density of deep capillary plexus) and D-dimers level.

Supplementary Fig. 46. The diagram for the correlation between VD S CC (superior vessel density of choriocapillaris) and D-dimers level.

Supplementary Fig. 47. The diagram for the correlation between VD N SCP (nasal vessel density of superficial capillary plexus) and D-dimers level.

Supplementary Fig. 48. The diagram for the correlation between VD N DCP (nasal vessel density of deep capillary plexus) and D-dimers level.

Supplementary Fig. 49. The diagram for the correlation between VD N CC (nasal vessel density of choriocapillaris) and D-dimers level.

Supplementary Fig. 50. The diagram for the correlation between VD I SCP (inferior vessel density of superficial capillary plexus) and D-dimers level.

Supplementary Fig. 51. The diagram for the correlation between VD I DCP (inferior vessel density of deep capillary plexus) and D-dimers level.

Supplementary Fig. 52. The diagram for the correlation between VD I CC (inferior vessel density of choriocapillaris) and D-dimers level.

Supplementary Fig. 53. The diagram for the correlation between VD T SCP (temporal vessel density of superficial capillary plexus) and D-dimers level.

Supplementary Fig. 54. The diagram for the correlation between VD T DCP (temporal vessel density of deep capillary plexus) and D-dimers level.

Supplementary Fig. 55. The diagram for the correlation between VD T CC (temporal vessel density of choriocapillaris) and D-dimers level.

Supplementary Fig. 56. The diagram for the correlation between mean VD SCP (vessel density of superficial capillary plexus) and D-dimers level.

Supplementary Fig. 57. The diagram for the correlation between mean VD DCP (vessel density of deep capillary plexus) and D-dimers level.

Supplementary Fig. 58. The diagram for the correlation between mean VD CC (vessel density of choriocapillaris) and D-dimers level.

Supplementary Fig. 59. The diagram for the correlation between FAZs (superficial foveal avascular zone) and D-dimers level.

Supplementary Fig. 60. The diagram for the correlation between FAZd (deep foveal avascular zone) and D-dimers level.

Supplementary Fig. 61. Histogram of IL-6 level.

Supplementary Fig. 62. Histogram of D-dimers level.

Supplementary Fig. 63. Histogram of saturation.

Supplementary Fig. 64. Histogram of VD F SCP (foveal vessel density of superficial capillary plexus).

Supplementary Fig. 65. Histogram of VD F DCP (foveal vessel density of deep capillary plexus).

Supplementary Fig. 66. Histogram of VD F CC (foveal vessel density of choriocapillaris).

Supplementary Fig. 67. Histogram of VD S SCP (superior vessel density of superficial capillary plexus).

Supplementary Fig. 68. Histogram of VD S DCP (superior vessel density of deep capillary plexus).

Supplementary Fig. 69. Histogram of VD S CC (superior vessel density of choriocapillaris).

Supplementary Fig. 70. Histogram of VD N SCP (nasal vessel density of superficial capillary plexus).

Supplementary Fig. 71. Histogram of VD N DCP (nasal vessel density of deep capillary plexus).

Supplementary Fig. 72. Histogram of VD N CC (nasal vessel density of choriocapillaris).

Supplementary Fig. 73. Histogram of VD I SCP (inferior vessel density of superficial capillary plexus).

Supplementary Fig. 74. Histogram of VD I DCP (inferior vessel density of deep capillary plexus).

Supplementary Fig. 75. Histogram of VD I CC (inferior vessel density of choriovcapillaris).

Supplementary Fig. 76. Histogram of VD T SCP (temporal vessel density of superficial capillary plexus).

Supplementary Fig. 77. Histogram of VD T DCP (temporal vessel density of deep capillary plexus).

Supplementary Fig. 78. Histogram of VD T CC (temporal vessel density of choriocapillaris).

Supplementary Fig. 79. Histogram of Mean VD SCP (vessel density of superficial capillary plexus).

Supplementary Fig. 80. Histogram of Mean VD DCP (vessel density of deep capillary plexus).

Supplementary Fig. 81. Histogram of Mean VD CC (vessel density of choriocapillaris).

Supplementary Fig. 82. Histogram of FAZs (superficial foveal avascular zone).

Supplementary Fig. 83. Histogram of FAZd (deep foveal avascular zone).

Supplementary Fig. 84. Normality distribution of VD F SCP in the category of saturation (foveal vessel density of superficial capillary plexus).

Supplementary Fig. 85. Normality distribution of VD F DCP in the category of saturation (foveal vessel density of deep capillary plexus).

Supplementary Fig. 86. Normality distribution of VD F CC in the category of saturation (foveal vessel density of choriocapillaris).

Supplementary Fig. 87. Normality distribution of VD S SCP in the category of saturation (superior vessel density of superficial capillary plexus).

Supplementary Fig. 88. Normality distribution of VD S DCP in the category of saturation (superior vessel density of deep capillary plexus).

Supplementary Fig. 89. Normality distribution of VD S CC in the category of saturation (superior vessel density of choriocapillaris).

Supplementary Fig. 90. Normality distribution of VD N SCP in the category of saturation (nasal vessel density of superficial capillary plexus).

Supplementary Fig. 91. Normality distribution of VD N DCP in the category of saturation (nasal vessel density of deep capillary plexus).

Supplementary Fig. 92. Normality distribution of VD N CC in the category of saturation (nasal vessel density of choriocapillaris).

Supplementary Fig. 93. Normality distribution of VD N DCP in the category of saturation (nasal vessel density of deep capillary plexus).

Supplementary Fig. 94. Normality distribution of VD I SCP in the category of saturation (inferior vessel density of superficial capillary plexus).

Supplementary Fig. 95. Normality distribution of VD I DCP in the category of saturation (inferior vessel density of deep capillary plexus).

Supplementary Fig. 96. Normality distribution of VD I CC in the category of saturation (inferior vessel density of choriocapillaris).

Supplementary Fig. 97. Normality distribution of VD T SCP in the category of saturation (temporal vessel density of superficial capillary plexus).

Supplementary Fig. 98. Normality distribution of VD T DCP in the category of saturation (temporal vessel density of deep capillary plexus).

Supplementary Fig. 99. Normality distribution of VD T CC in the category of saturation (temporal vessel density of choriocapillaris).

Supplementary Fig. 100. Normality distribution of mean VD SCP in the category of saturation (vessel density of superficial capillary plexus).

Supplementary Fig. 101. Normality distribution of mean VD DCP in the category of saturation (vessel density of deep capillary plexus).

Supplementary Fig. 102. Normality distribution of FAZs (superficial foveal avascular zone) in the category of saturation.

Supplementary Fig. 103. Normality distribution of FAZd (deep foveal avascular zone) in the category of saturation.

Supplementary Fig. 104. Normality distribution of VD F SCP (foveal vessel density of superficial capillary plexus) in the category of D-dimers level.

Supplementary Fig. 105. Normality distribution of VD F DCP (foveal vessel density of deep capillary plexus) in the category of D-dimers level.

Supplementary Fig. 106. Normality distribution of VD F CC (foveal vessel density of choriocapillaris) in the category of D-dimers level.

Supplementary Fig. 107. Normality distribution of VD F DCP (foveal vessel density of deep capillary plexus) in the category of D-dimers level.

Supplementary Fig. 108. Normality distribution of VD S DCP (superior vessel density of deep capillary plexus) in the category of D-dimers level.

Supplementary Fig. 109. Normality distribution of VD S CC (superior vessel density of choriocapillaris) in the category of D-dimers level.

Supplementary Fig. 110. Normality distribution of VD N SCP (nasal vessel density of superficial capillary plexus) in the category of D-dimers level.

Supplementary Fig. 111. Normality distribution of VD N DCP (nasal vessel density of deep capillary plexus) in the category of D-dimers level.

Supplementary Fig. 112. Normality distribution of VD N CC (nasal vessel density of choriocapillaris) in the category of D-dimers level.

Supplementary Fig. 113. Normality distribution of VD I SCP (inferior vessel density of superficial capillary plexus) in the category of D-dimers level.

Supplementary Fig. 114. Normality distribution of VD I DCP (inferior vessel density of deep capillary plexus) in the category of D-dimers level.

Supplementary Fig. 115. Normality distribution of VD I CC (inferior vessel density of choriocapillaris) in the category of D-dimers level.

Supplementary Fig. 116. Normality distribution of VD T SCP (temporal vessel density of superficial capillary plexus) in the category of D-dimers level.

Supplementary Fig. 117. Normality distribution of VD T DCP (temporal vessel density of deep capillary plexus) in the category of D-dimers level.

Supplementary Fig. 118. Normality distribution of VD T CC (temporal vessel density of choriocapillaris) in the category of D-dimers level.

Supplementary Fig. 119. Normality distribution of mean VD SCP (vessel density of superficial capillary plexus) in the category of D-dimers level.

Supplementary Fig. 120. Normality distribution of mean VD DCP (vessel density of deep capillary plexus) in the category of D-dimers level.

Supplementary Fig. 121. Normality distribution of mean VD CC (vessel density of choriocapillaris) in the category of D-dimers level.

Supplementary Fig. 122 Normality distribution of FAZs (superficial foveal avascular zone) in the category of D-dimers level.

Supplementary Fig. 123. Normality distribution of FAZd (deep foveal avascular zone) in the category of D-dimers level.

Supplementary Fig. 124. Histogram for VD F SCP (foveal vessel density of superficial capillary plexus) in 2 groups of IL-6 level.

Supplementary Fig. 125. Histogram for VD F DCP (foveal vessel density of deep capillary plexus) in 2 groups of IL-6 level.

Supplementary Fig. 126. Histogram for VD F CC (vessel density of choriocapillaris) in 2 groups of IL-6 level.

Supplementary Fig. 127. Histogram for VD S SCP (foveal vessel density of superficial capillary plexus) in 2 groups of IL-6 level.

Supplementary Fig. 128. Histogram for VD S DCP (superior vessel density of deep capillary plexus) in 2 groups of IL-6 level.

Supplementary Fig. 129. Histogram for VD S CC (superior vessel density of choriocapillaris) in 2 groups of IL-6 level.

Supplementary Fig. 130. Histogram for VD N SCP (nasal vessel density of superficial capillary plexus) in 2 groups of IL-6 level.

Supplementary Fig. 131. Histogram for VD N DCP (nasal vessel density of deep capillary plexus) in 2 groups of IL-6 level.

Supplementary Fig. 132. Histogram for VD N CC (nasal vessel density of choriocapillaris) in 2 groups of Interleukin 6 (IL 6).

Supplementary Fig. 133. Histogram for VD I SCP (inferior vessel density of superficial capillary plexus) in 2 groups of IL-6 level.

Supplementary Fig. 134. Histogram for VD I DCP (inferior vessel density of deep capillary plexus) in 2 groups of IL-6 level.

Supplementary Fig. 135 Histogram for VD I CC (inferior Vessel density of choriocapillaris) in 2 groups of IL-6 level. Supplementary Fig. 136. Histogram for VD T SCP (temporal vessel density of superficial capillary plexus) in 2 groups of IL-6 level.

Supplementary Fig. 137. Histogram for VD T DCP (temporal vessel density of deep capillary plexus) in 2 groups of IL-6 level.

Supplementary Fig. 138. Histogram for VD T CC (temporal vessel density of choriocapillaris) in 2 groups of IL-6 level.

Supplementary Fig. 139. Histogram for mean VD SCP (mean vessel density of superficial capillary plexus) in 2 groups of IL-6 level.

Supplementary Fig. 140. Histogram for mean VD DCP (mean vessel density of deep capillary plexus) in 2 groups of IL-6 level.

Supplementary Fig. 141. Histogram for mean VD CC (mean vessel density of choriocapillaris) in 2 groups of IL-6 level.

Supplementary Fig. 142. Histogram for FAZs (superficial foveal avascular zone) in 2 groups of IL-6 level.

Supplementary Fig. 143. Histogram for FAZd (deep foveal avascular zone) in 2 groups of IL-6 level.

Data availability

The datasets generated and/or analyzed during the current study are available from the corresponding author on reasonable request.

Consent for publication

Not applicable.

ORCID iDs

References

- Perico L, Benigni A, Casiraghi F, Ng LFP, Renia L, Remuzzi G. Immunity, endothelial injury and complement-induced coagulopathy in COVID-19. Nat Rev Nephrol. 2021;17(1):46–64. doi:10.1038/s41581-020-00357-4
- Patel A, Charani E, Ariyanayagam D, et al. New-onset anosmia and ageusia in adult patients diagnosed with SARS-CoV-2 infection. Clin Microbiol Infect. 2020;26(9):1236–1241. doi:10.1016/j.cmi.2020.05.026
- Romero-Sánchez CM, Díaz-Maroto I, Fernández-Díaz E, et al. Neurologic manifestations in hospitalized patients with COVID-19: The ALBA-COVID registry. Neurology. 2020;95(8):e1060–e1070. doi:10.1212/WNL. 000000000009937
- Dockery DM, Rowe SG, Murphy MA, Krzystolik MG. The ocular manifestations and transmission of COVID-19: Recommendations for prevention. *J Emerg Med*. 2020;59(1):137–140. doi:10.1016/j.jemermed. 2020.04.060
- Suresh Kumar VC, Mukherjee S, Harne PS, et al. Novelty in the gut: A systematic review and meta-analysis of the gastrointestinal manifestations of COVID-19. BMJ Open Gastroenterol. 2020;7(1):e000417. doi:10.1136/bmjgast-2020-000417
- Jin X, Lian JS, Hu JH, et al. Epidemiological, clinical and virological characteristics of 74 cases of coronavirus-infected disease 2019 (COVID-19) with gastrointestinal symptoms. Gut. 2020;69(6):1002– 1009. doi:10.1136/gutjnl-2020-320926
- Shi S, Qin M, Shen B, et al. Association of cardiac injury with mortality in hospitalized patients with COVID-19 in Wuhan, China. *JAMA Cardiol*. 2020;5(7):802. doi:10.1001/jamacardio.2020.0950
- Wang X, Tang G, Liu Y, et al. The role of IL-6 in coronavirus, especially in COVID-19. Front Pharmacol. 2022;13:1033674. doi:10.3389/fphar.2022.1033674
- Hoffmann M, Kleine-Weber H, Schroeder S, et al. SARS-CoV-2 cell entry depends on ACE2 and TMPRSS2 and is blocked by a clinically proven protease inhibitor. *Cell*. 2020;181(2):271–280.e8. doi:10.1016/j. cell.2020.02.052
- Banderas García S, Aragón D, Azarfane B, et al. Persistent reduction of retinal microvascular vessel density in patients with moderate and severe COVID-19 disease. *BMJ Open Ophthalmol*. 2022;7(1):e000867. doi:10.1136/bmjophth-2021-000867
- Zhou F, Yu T, Du R, et al. Clinical course and risk factors for mortality of adult inpatients with COVID-19 in Wuhan, China: A retrospective cohort study. *Lancet*. 2020;395(10229):1054–1062. doi:10.1016/S0140-6736(20)30566-3
- Kal M, Winiarczyk M, Głuszek S, Mackiewicz J. Choroidal thickness in lamellar macular holes. *Graefes Arch Clin Exp Ophthalmol*. 2021; 259(3):653–659. doi:10.1007/s00417-020-04922-2
- Marinho PM, Marcos AAA, Romano AC, Nascimento H, Belfort R. Retinal findings in patients with COVID-19. Lancet. 2020;395(10237):1610. doi:10.1016/S0140-6736(20)31014-X
- Schnichels S, Rohrbach JM, Bayyoud T, Thaler S, Ziemssen F, Hurst J. Can SARS-CoV-2 infect the eye? An overview of the receptor status in ocular tissue. Ophthalmologe. 2021;118(Suppl 1):81–84. doi:10.1007/ s00347-020-01281-5
- Kal M, Winiarczyk M, Cieśla E, et al. Retinal microvascular changes in COVID-19 bilateral pneumonia based on optical coherence tomography angiography. J Clin Med. 2022;11(13):3621. doi:10.3390/jcm 11133621
- Kal M, Winiarczyk M, Zarębska-Michaluk D, et al. Long-term effect of SARS-CoV-2 infection on the retinal and choroidal microvasculature. J Clin Med. 2023;12(7):2528. doi:10.3390/jcm12072528

- Flisiak R, Parczewski M, Horban A, et al. Management of SARS-CoV-2 infection: Recommendations of the Polish Association of Epidemiologists and Infectiologists. Annex No. 2 as of October 13, 2020. Pol Arch Intern Med. 2020;130(10):915–918. doi:10.20452/pamw.15658
- Flisiak R, Horban A, Jaroszewicz J, et al. Diagnosis and therapy of SARS-CoV-2 infection: Recommendations of the Polish Association of Epidemiologists and Infectiologists as of November 12, 2021. Annex No. 1 to the Recommendations of April 26, 2021. Pol Arch Intern Med. 2021; 131(11):16140. doi:10.20452/pamw.16140
- López Reboiro ML, Suárez Fuentetaja R, Gutiérrez López R, et al. Role of lupus anticoagulant and von Willebrand factor in chronic reactive endotheliitis in COVID-19. J Infect. 2021;82(6):e27–e28. doi:10.1016/j. jinf.2021.03.006
- 20. Padhy SK, Dcruz RP, Kelgaonkar A. Paracentral acute middle maculopathy following SARS-CoV-2 infection: The D-dimer hypothesis. BMJ Case Rep. 2021;14(3):e242043. doi:10.1136/bcr-2021-242043
- 21. Virgo J, Mohamed M. Paracentral acute middle maculopathy and acute macular neuroretinopathy following SARS-CoV-2 infection. *Eye.* 2020;34(12):2352–2353. doi:10.1038/s41433-020-1069-8
- Naughton A, Ong AY, Gkika T, Downes S. Bilateral paracentral acute middle maculopathy in a SARS-CoV-2-positive patient. *Postgrad Med J*. 2022;98(e2):e105–e106. doi:10.1136/postgradmedj-2021-140500
- Ozsaygılı C, Bayram N, Ozdemir H. Cilioretinal artery occlusion with paracentral acute middle maculopathy associated with COVID-19. *Indian J Ophthalmol*. 2021;69(7):1956. doi:10.4103/ijo.IJO_563_21
- Kal M, Winiarczyk M, Mackiewicz J, et al. The effect of reduced oxygen saturation on retinal microvascularization in COVID-19 patients with bilateral pneumonia based on optical coherence tomography study. J Pers Med. 2022;12(11):1824. doi:10.3390/jpm12111824
- 25. Hommer N, Kallab M, Sim YC, et al. Effect of hyperoxia and hypoxia on retinal vascular parameters assessed with optical coherence tomography angiography. *Acta Ophthalmol*. 2022;100(6):e1272–e1279. doi:10.1111/aos.15077
- 26. Werkmeister RM, Schmidl D, Aschinger G, et al. Retinal oxygen extraction in humans. *Sci Rep.* 2015;5(1):15763. doi:10.1038/srep15763
- Hagag AM, Pechauer AD, Liu L, et al. OCT angiography changes in the 3 parafoveal retinal plexuses in response to hyperoxia. Ophthalmol Retina. 2018;2(4):329–336. doi:10.1016/j.oret.2017.07.022

- 28. Conrath J, Giorgi R, Ridings B, Raccah D. Metabolic factors and the foveal avascular zone of the retina in diabetes mellitus. *Diabetes Metab.* 2005;31(5):465–470. doi:10.1016/S1262-3636(07)70217-3
- Samara WA, Say EAT, Khoo CTL, et al. Correlation of foveal avascular zone size with foveal morphology in normal eyes using optical coherence tomography angiography. *Retina*. 2015;35(11):2188–2195. doi:10.1097/IAE.0000000000000847
- Guemes-Villahoz N, Burgos-Blasco B, Vidal-Villegas B, et al. Reduced retinal vessel density in COVID-19 patients and elevated D-dimer levels during the acute phase of the infection. *Med Clin (Barc)*. 2021; 156(11):541–546. doi:10.1016/j.medcli.2020.12.006
- Guemes-Villahoz N, Burgos-Blasco B, Vidal-Villegas B, et al. Reduced macular vessel density in COVID-19 patients with and without associated thrombotic events using optical coherence tomography angiography. *Graefes Arch Clin Exp Ophthalmol*. 2021;259(8):2243–2249. doi:10.1007/s00417-021-05186-0
- 32. Glass J, Robinson R, Lee TJ, Sharma A, Sharma S. Interleukin-6 transsignaling mediated regulation of paracellular permeability in human retinal endothelial cells. *Int J Transl Med*. 2021;1(2):137–153. doi:10.3390 //iitm1020010
- Mesquida M, Drawnel F, Lait PJ, et al. Modelling macular edema: The effect of IL-6 and IL-6R blockade on human blood–retinal barrier integrity in vitro. *Trans Vis Sci Tech*. 2019;8(5):32. doi:10.1167/tvst.8.5.32
- Park YJ, Acosta D, Vassell R, et al. D-dimer and CoV-2 spike-immune complexes contribute to the production of PGE2 and proinflammatory cytokines in monocytes. *PLoS Pathog*. 2022;18(4):e1010468. doi:10.1371/journal.ppat.1010468
- Levi M, Van Der Poll T, Büller HR. Bidirectional relation between inflammation and coagulation. *Circulation*. 2004;109(22):2698–2704. doi:10.1161/01.CIR.0000131660.51520.9A
- Gris JC, Perez-Martin A, Quéré I, Sotto A. COVID-19 associated coagulopathy: The crowning glory of thrombo-inflammation concept. *Anaesth Crit Care Pain Med*. 2020;39(3):381–382. doi:10.1016/j.accpm. 2020.04.013